




Identification of the average and local boundary condition of heat transfer during cooling with a water spray under surface boiling

Elżbieta Jasiewicz* , Beata Hadała , Zbigniew Malinowski 

AGH University of Science and Technology, Faculty of Metals Engineering and Industrial Computer Science, Department of Heat Engineering and Environment Protection, al. Mickiewicza 30, 30-059 Krakow, Poland.

Abstract

The study determined the local and average heat transfer coefficient and the heat flux on the surface of a cylinder cooled with a water nozzle. The inverse method was used to identify the heat transfer coefficient. An objective function was defined to determine the distance between the measured and calculated temperatures. Two models describing the heat transfer coefficient on the cooled surface were considered. The first model described changes in the heat transfer coefficient as a function of the sample radius and cooling time, and the second one assumed the dependence of the heat transfer coefficient solely on time. Numerical simulations showed significant differences in the determined heat transfer coefficients depending on the adopted model of the boundary condition. The performed tests included experimental temperature measurements at selected points of the sensor, numerical simulations of temperature changes, and the inverse solution.

Keywords: water spray cooling, heat transfer coefficient, heat flux, inverse problem for the heat conduction equation

1. Introduction

Fluid-based heat removal systems are attracting increasing interest for cooling electronics, laser devices, and in the energy industry (Silk et al., 2008). This method allows high values of the heat transfer coefficient on the surface of the cooled object to be achieved and the maintenance of the required temperature of the cooled surface, thus increasing cooling efficiency.

Numerical simulations enable the determination of an appropriate cooling rate at low cost, when the boundary conditions on the surface of the cooled material are known (Sun et al., 2002). A significant improvement in

the obtained results is achieved by applying the boundary condition in the form of heat transfer coefficient distribution (Edalatpour et al., 2011). There are methods for measuring the local heat transfer coefficient, such as the mass transfer method or the method using liquid crystals to measure the surface temperature. However, these methods cannot be applied to high-temperature processes. Another group of methods commonly used to determine the heat transfer coefficient during water cooling is based on solutions to the problem of the inverse heat conduction equation. In this case, the heat transfer coefficient on the surface of the cooled material is determined from the minimum of the objective function that defines

* Corresponding author: jasiewicz@agh.edu.pl

ORCID ID's: 0000-0002-5412-4872 (E. Jasiewicz), 0000-0001-9904-7885 (B. Hadała), 0000-0003-2862-7588 (Z. Malinowski)
© 2020 Authors. This is an open access publication, which can be used, distributed and reproduced in any medium according to the Creative Commons CC-BY 4.0 License requiring that the original work has been properly cited.

the differences between the measured and calculated temperature values. Inverse solutions of the one-dimensional problem (Bellerová et al., 2012; Volle et al., 2009) and the two-dimensional problem (Cebo-Rudnicka et al., 2016; Kim & Oh, 2001) of heat conduction were used to obtain an average value of the heat flux on the cooled surface.

The growing demand for the development of advanced cooling systems and modeling of microstructure development processes requires the provision of a local heat transfer coefficient. One of the first attempts to determine the heat transfer coefficient distribution on the surface were the results of the temperature readings, presented by the authors of the publications (Huang & Wang, 1999; Zhou et al., 2012), determined on the basis of computer simulations. Local changes in the heat transfer coefficient obtained on the basis of the actual measurement of the temperature change of the cooled surface are presented in the studies (Hadała et al., 2019). The identification of the boundary condition was made for cooling metals by water spray, using the inverse solution, with a three-dimensional model of heat conduction. The models of boundary conditions presented in the above-mentioned works enable the definition of the local heat transfer coefficient depending on the surface temperature and water pressure. The list of symbols used in the paper has been given in Table 1.

The main purpose of the article was to identify the boundary conditions of heat transfer (heat transfer coefficient and heat flux) on the cooled surface of a cylindrical sensor cooled by water spray. The HTC and HF values were computed from the two models of the

boundary conditions implemented in the inverse solution. The accuracy of the boundary condition models was assessed and compared.

2. Heat conduction model

The identification of the boundary condition for cooling metals using water spray was carried out on the basis of temperature measurements of the cooled cylinder and calculations of the temperature field from the heat conduction equation:

$$\rho c_p(t) \frac{\partial t(r, y, \tau)}{\partial \tau} = \frac{1}{r} \frac{\partial}{\partial r} \left[\lambda(t) r \frac{\partial t(r, y, \tau)}{\partial r} \right] + \frac{\partial}{\partial y} \left[\lambda(t) \frac{\partial t(r, y, \tau)}{\partial y} \right] \quad (1)$$

assuming that:

$$(0 < r < R; 0 < y < h; \tau > 0)$$

The solution of equation (1) was obtained using the finite element method, which transforms equation (1) into a system of algebraic linear equations (Zienkiewicz & Taylor, 2000):

$$K_{ij} T_j + C_{ij} \frac{\partial T_j}{\partial \tau} = B_i \quad (2)$$

Table 1. Nomenclature

c_p	specific heat [J/(kg·K)]	t_m	cooling medium temperature [°C]
h	sensor height [m]	t_s	cooled surface temperature [°C]
H_i	shape functions	$\Delta\tau$	time increment
L_o	outer casing diameter [m]	ε_c	the emissivity of the sensor surface
L_p	distance between sensor and casing [m]	ε_o	the emissivity of the casing surface
Pr	Prandtl number	η	dimensionless time
R_{\max}	maximum radius of the sensor with casing [m]	ϑ	dimensionless sensor radius
Ra	Rayleigh number	λ	thermal conductivity [W/(m·K)]
r, y	cylindrical coordinates	λ_p	thermal conductivity of air [W/(m·K)]
T_c	temperature of the sensor side surface [K]	ρ	density [kg/m ³]
T_o	casing surface temperature [K]	σ	Stefan–Boltzmann radiation constant [W/(m ² ·K ⁴)]
T_{ot}	ambient temperature [K]	τ	time [s]
t	temperature [°C]		
t_b	temperature of the outer surface of the side casing [°C]		
t_{ij}^o	sensor temperature calculated by the heat conduction model in position and time [°C]		
t_{ij}^z	temperature obtained as a result of measurement in the sensor over time τ [°C]		
		Abbreviations	
		HF	heat flux [kW/m ²]
		HTC	heat transfer coefficient [W/(m ² ·K)]

For one element, matrices K_{ij} , C_{ij} , and vector B_i take the form:

$$K_{ij} = \sum \int_{\Omega_e} \lambda \left(\frac{\partial H_i}{\partial r} \frac{\partial H_j}{\partial r} + \frac{\partial H_i}{\partial z} \frac{\partial H_j}{\partial z} \right) r d\Omega_e + \sum \int_{S_e} r H_i H_j \alpha dS_e \quad (3)$$

$$C_{ij} = \sum \int_{\Omega_e} \rho c H_i H_j r d\Omega_e \quad (4)$$

$$B_i = \sum \int_{S_e} H_i (\alpha T_a) r dS_e \quad (5)$$

The description of the FEM method used to solve the equation (1) is given in (Telejko & Malinowski, 2004). Accuracy tests of the applied FEM solution for modeling the temperature field of an axisymmetric sensor with a casing were carried out, obtaining a satisfactory accuracy and the computation time (Cebo-Rudnicka et al., 2016).

3. Inverse solution to the problem of heat conduction

The boundary condition on the water-cooled surface was sought for in the form of two functions:

- dependent on location and time, enabling the determination of the local value of the boundary condition (variant 1):

$$\dot{q} = \alpha(r, \tau)(t_s - t_m) \quad (6)$$

- depending on time, the HTC value on the entire cooled surface is the same, but it changes over time (variant 2):

$$\dot{q} = \alpha(\tau)(t_s - t_m) \quad (7)$$

In both variants, the general form of the function approximating the change of the HTC with time was adopted. The objective function was adopted in the form of an error norm:

$$E(p_i) = \sum_{i=1}^n \sum_{j=1}^m \left[\frac{1}{\sqrt{1 + \left(\frac{\Delta t_{ij}^z}{\Delta \tau} \right)^2}} (t_{ij}^z(\tau) - t_{ij}^o(p_i, \tau)) \right]^2 \quad (8)$$

The error norm (8) defines the distance between computed and measured temperatures always normal to the measured temperature curve. The dimensionless

term preceding the temperature difference defines the cosine of the normal to the measured temperature curve. The term $\Delta t_{ij}^z / \Delta \tau$ defines a tangent of the inclination of the measured temperature t^z at a sampling point ij . The values of unknown parameters p_i were determined by minimizing the objective function. The variable metric method was used (Kręglewski et al., 1984), which uses the BFGS algorithm (Broyden, 1970; Fletcher, 1970; Goldfarb, 1970; Shanno, 1970). The objective function derivatives with respect to the unknown p_i parameters were estimated numerically.

It has been assumed that the distribution of the HTC along the sample radius can be approximated with the third-degree polynomial. Since at $r = 0$ the temperature derivative is equal to zero, the distribution of the HTC along the sensor radius (variant 1) was determined using the reduced Hermitian shape functions:

$$\alpha(r, \tau) = (1 - 3\vartheta^2 + 2\vartheta^3)F_1(\tau) + (3\vartheta^2 - 2\vartheta^3)F_2(\tau) + R_{\max}(\vartheta^3 - \vartheta^2)F_3(\tau) \quad (9)$$

The dimensionless radius of the sensor was calculated from the formula:

$$\vartheta = \frac{r}{R_{\max}} \quad (10)$$

The $F_1(\tau)$ parameter determines the value of the HTC in the sensor axis ($r = 0$), while the $F_2(\tau)$ parameter defines the value of this coefficient for $r = R_{\max}$. Parameter F_3 defines the derivative of this coefficient with respect to the radius for $r = R_{\max}$. The distribution of the parameters $F_1(\tau)$, $F_2(\tau)$ and $F_3(\tau)$ over time was approximated by the following functions (Cebo-Rudnicka et al., 2016):

$$F_1(\tau) = \sum_{i=1}^4 H_i p_{1i}(\tau_i) \quad (11)$$

$$F_2(\tau) = \sum_{i=1}^4 H_i p_{2i}(\tau_i) \quad (12)$$

$$F_3(\tau) = \sum_{i=1}^4 H_i p_{3i}(\tau_i) \quad (13)$$

In the case of variant 2, it was assumed that the HTC value on the entire cooled surface is the same, but it changes over time. Taking this assumption into account, the HTC during sample cooling was determined using the polynomial:

$$\alpha(\tau) = F_1(\tau) \quad (14)$$

Parameter $F_1(\tau)$ determines the value of the HTC on the sample surface.

The function $F_1(\tau)$ was approximated by polynomials:

$$F_1(\tau) = \sum_{i=1}^4 H_i p_i(\tau_i) \quad (15)$$

In variants 1 and 2, the cooling time was divided into periods in which $\tau \in (\tau_1, \tau_2)$. The third degree Hermite polynomial was used to approximate the HTC distribution over a period (Cebo-Rudnicka et al., 2016):

$$H_1 = \frac{(1-\eta)(9\eta^2-1)}{16} \quad (16)$$

$$H_2 = \frac{9(1-3\eta)(1-\eta^2)}{16} \quad (17)$$

$$H_3 = \frac{9(1+3\eta)(1-\eta^2)}{16} \quad (18)$$

$$H_4 = \frac{(1+\eta)(9\eta^2-1)}{16} \quad (19)$$

where η – dimensionless time:

$$\eta = \frac{2\tau - \tau_1 - \tau_2}{\tau_2 - \tau_1} \quad (20)$$

The set of unknown parameters p_{1i} , p_{2i} and p_{3i} collected in the p_i vector was determined by minimizing the objective function. This vector consists of the value of the HTC in the nodes of the approximation of the HTC in time. In the case of variant 1, the set of p_i parameters determines the change of the HTC on the cooled surface as a function of time and sensor radius. In the case of calculations for variant 2, the set of p_i parameters, which gives the minimum of the objective function, determines the change of the HTC on the cooled surface as a function of time only.

4. Experimental research

The temperature measurement stand consisted of three main parts: an electric resistance furnace, a cooling chamber with a nozzle and a water tank (Fig. 1). A cylindrical sensor made of Inconel 600 alloy with a diameter of 20 mm was tested. The sensor was surrounded by a casing made of Inconel 600 alloy with air between the casing and the sensor (Fig. 2). The sensor with the casing was heated in a furnace to 900°C, and then, by means of an automatic feeder, was transferred to the cooling chamber, where it was cooled by a spray of water. In the chamber, the cooled sensor was placed in a vertical position, perpendicular to the water stream.

Water was sprayed from one MNQ 1040 T1SH (*Steel work nozzles*, n.d.) nozzle, the distance between the nozzle and the surface was 50 mm.

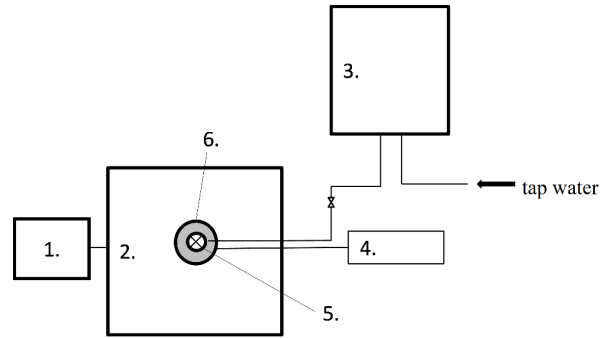


Fig. 1. Scheme of the measuring stand: 1 – electric furnace; 2 – chamber; 3 – water tank; 4 – temperature measurement system; 5 – nozzle; 6 – sensor with thermocouples

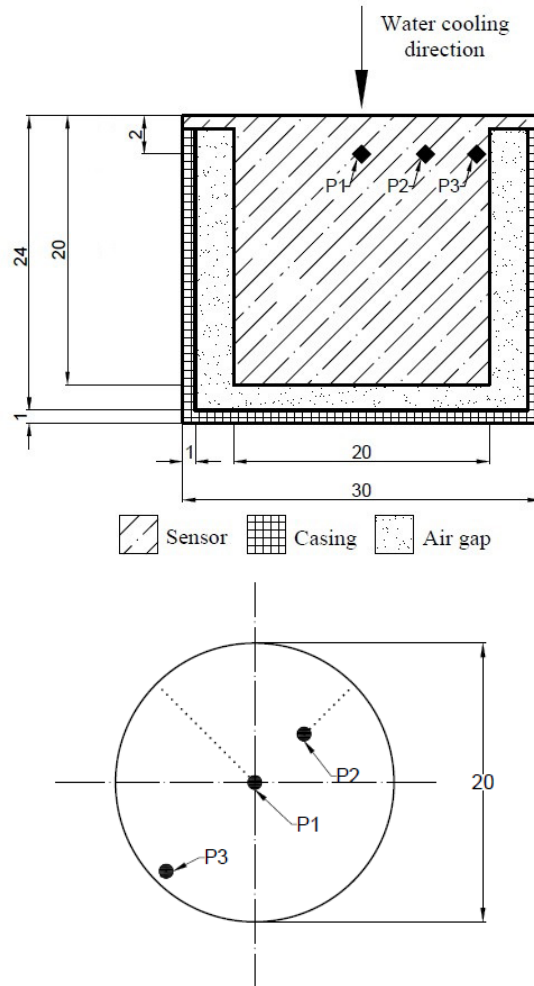


Fig. 2. Scheme of the sensor with the location of thermocouples (P1, P2, P3)

The temperature of the sensor was measured at 3 points using NiCr-NiAl (type K) thermocouples with a diameter of 1 mm. Thermocouples P1, P2, and P3 were

placed 2 mm below the cooled surface (Fig. 2). The temperature was recorded with the measuring system with a frequency of 0.1 s. The accuracy class of the temperature recording system was 0.2%. The accuracy of the thermocouples guaranteed by the manufacturer was $\pm 0.4\%$ of the measured temperature value. The selection of measuring points resulted mainly from the assumption of symmetrical cooling of the surface by the nozzle. The coolant was fed from above under a pressure of 0.05 MPa.

5. Numerical calculations

Numerical calculations identifying the HTC were performed using a program based on solving the inverse boundary problem for the heat conduction equation (1). The calculations were carried out on the assumption that thermal conductivity and specific heat of the sensor material change with the temperature. It was assumed that the density of the sensor material was $\rho = 8470 \text{ kg/m}^3$ (PROMAT), and the emissivity of the material was 0.2. The applied division into elements is shown in Figure 3.

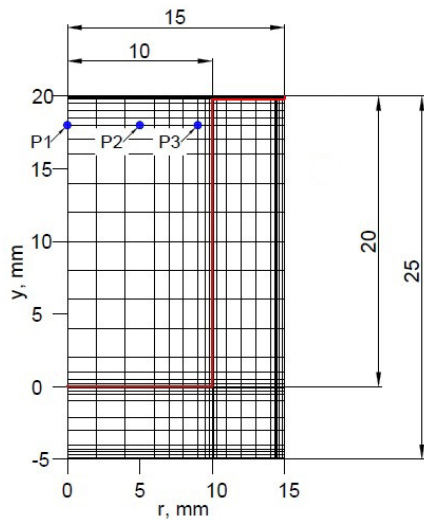


Fig. 3. Finite element mesh with the location of thermocouples

The heat flux exchanged between the side surface of the sensor, and the inner surface of the casing was calculated from the boundary condition, taking into account the heat exchange due to radiation and convection (Cebo-Rudnicka et al., 2016):

$$\dot{q} = \sigma \cdot \frac{T_c^4 - T_o^4}{\frac{1}{\varepsilon_c} + \frac{1}{\varepsilon_o} - 1} + \frac{\lambda_p}{L_p} \cdot 0.22 \cdot \left(\frac{Pr}{0.2 + Pr} \cdot Ra \right)^{0.28} \cdot \left(\frac{h}{L_p} \right)^{-\frac{1}{4}} \cdot (T_c - T_o) \quad (21)$$

The boundary condition on the lower outer surface of the casing was calculated from the equation (Cebo-Rudnicka et al., 2016):

$$\dot{q}_d = \sigma \cdot \varepsilon_o \cdot (T_o^4 - T_{ot}^4) + \frac{\lambda_p}{L_o} \cdot 0.474 \cdot Ra^{0.25} \cdot Pr^{0.047} \cdot (T_o - T_{ot}) \quad (22)$$

The thermophysical properties of air and the criterion number of similarities appearing in equations (21, 22) were determined for the average fluid temperature.

A boundary condition was defined on the outer surface of the casing in the form (Malinowski, 2005):

$$\alpha_b = 0.117487t_b - 0.466701 \cdot 10^{-3} t_b^2 + 6.932216 \cdot 10^{-7} t_b^3 - 3.661325 \cdot 10^{-10} t_b^4 \quad (23)$$

6. Identification of the heat transfer coefficient and heat flux

The numerical calculations performed made it possible to determine the local values of HTC and HF on the cooled surface (variant 1) and the average values of HTC and HF on this surface (variant 1 and variant 2). The local values of HTC and HF were determined at points located along the sensor radius: P1 = 1.58 mm, P2 = 5.58 mm, and P3 = 9.84 mm (Fig. 3). The average values of HTC and HF were determined in the areas with a cooled surface: S1, S2, and S3, defined by the corresponding radii, respectively: $r_1 = 1.58 \text{ mm}$, $r_2 = 5.58 \text{ mm}$, $r_3 = 9.84 \text{ mm}$ (Fig. 4).

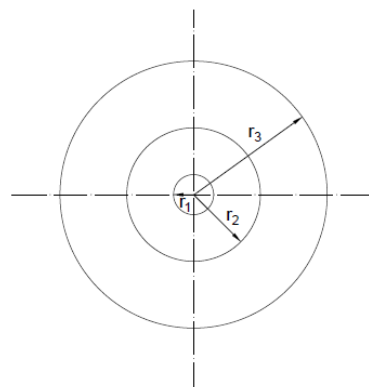


Fig. 4. Diagram showing the areas of the cooled surface of the sensor for which the average values of HTC and HF were determined

The calculation results presented in the form of curves in Figures 5–8 indicate significantly different changes in HTC and HF at points P1, P2, and P3. The highest values of HTC and HF were obtained at point

P1, and the lowest at point P3. Thus, the area of the most intense cooling occurs in the sensor axis, and the cooling intensity decreases with increasing distance from the sensor axis.

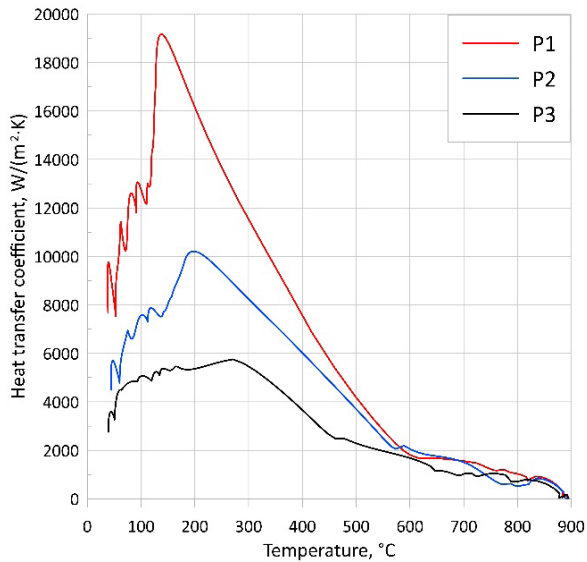


Fig. 5. The dependence of HTC in 3 points on the surface temperature (variant 1)

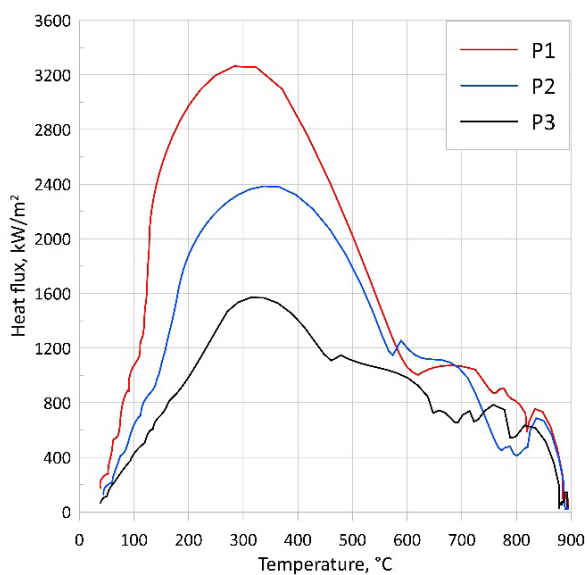


Fig. 6. The dependence of HF at 3 points on the surface temperature (variant 1)

The courses of HTC and HF changes depending on time and temperature at points P1, P2, and P3 (Figs. 5–8) has allowed observing three characteristic boiling phases on the cooled surface: film boiling, transient boiling and nucleate boiling. Film boiling occurred at the initial stage of cooling, in which the degree of liquid overheating above the saturation temperature was high. The film boiling area is char-

acterized by relatively low HTC and HF values due to the vapor film formed on the surface, which separates the liquid from the cooled surface, thus limiting heat transfer. The film boiling on the surface ended after about 12 seconds from the beginning of cooling (Figs. 7 and 8), when the temperature of the cooled surface reached approximately 600°C. Below this temperature, there was a sharp increase in HTC and HF. This was due to the transient boiling phase in which the liquid directly wets the surface. After reaching the maximum HF value, the nucleate boiling phase begins, in which the vapor bubbles begin to gradually disappear as the surface temperature decreases until the surface temperature is below the saturation temperature of the liquid, at which the boiling process ceases.

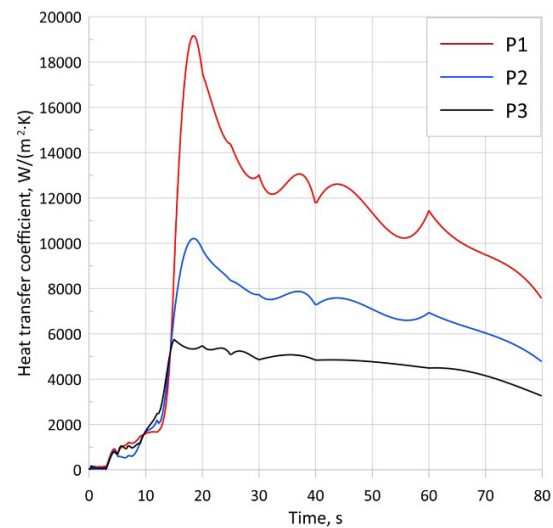


Fig. 7. The HTC evolution with time in 3 points (variant 1)

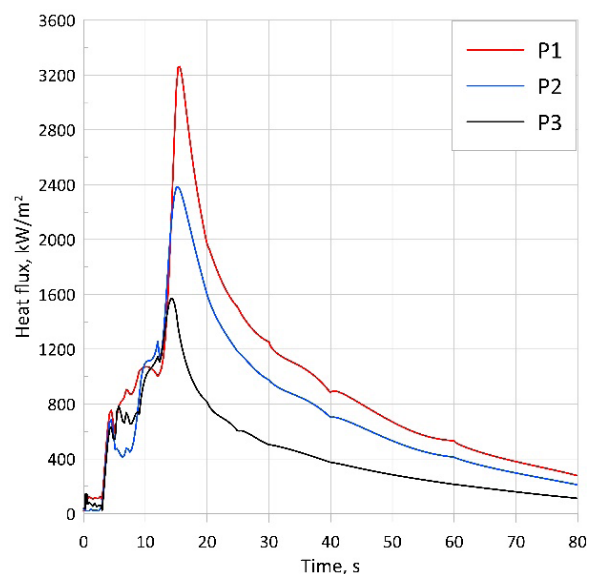


Fig. 8. The HF evolution with time in 3 points (variant 1)

The highest average value of HTC (Fig. 9) and HF (Fig. 10) for all phases of the boiling was obtained on the surface of radius r_1 . The HTC maximum in this area was $19,395 \text{ W}/(\text{m}^2\cdot\text{K})$. Along with increasing the averaging area, the maximum average HTC values decreased by about $5000 \text{ W}/(\text{m}^2\cdot\text{K})$ for the area with radius r_2 and by about $10,000 \text{ W}/(\text{m}^2\cdot\text{K})$ for the area with radius r_3 . It also shifted in relation to the higher values of the surface temperature with the increase of the averaging area. A similar relationship is also observed in the case of average HF values (Fig. 10). The highest value was obtained in the area of radius r_1 – it was over $3200 \text{ kW}/\text{m}^2$. In the area of radius r_2 , this value decreased by over $400 \text{ kW}/\text{m}^2$, and in the area of radius r_3 – by about $1000 \text{ kW}/\text{m}^2$, in relation to the maximum of the average HF value in the area of radius r_1 .

The course of the change in the average values of HTC and HF, determined using the model designated as variant 2, is similar in terms of the value of the film boiling in relation to the results obtained in the same area with the use of variant 1 (Figs. 9 and 10). However, the film boiling phase ends approximately 40°C below the temperature observed for variant 1. There is also a visible shift of the maximum HTC to the temperature of 125°C , the lowest in relation to all analyzed cases.

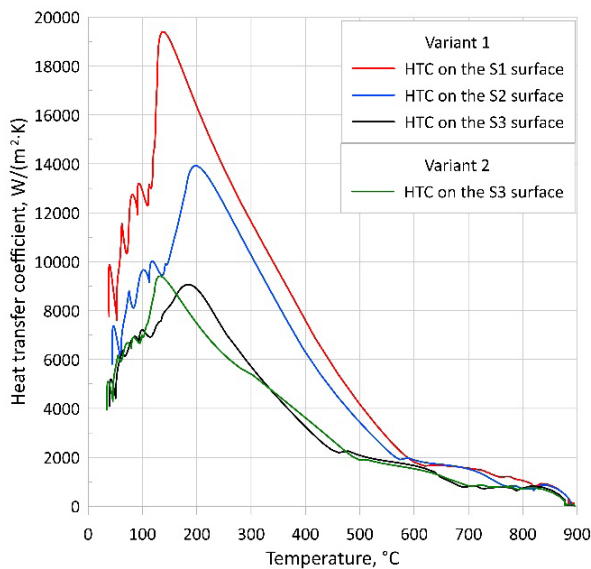


Fig. 9. The average values of HTC, obtained in particular areas depending on the temperature of the cooled surface

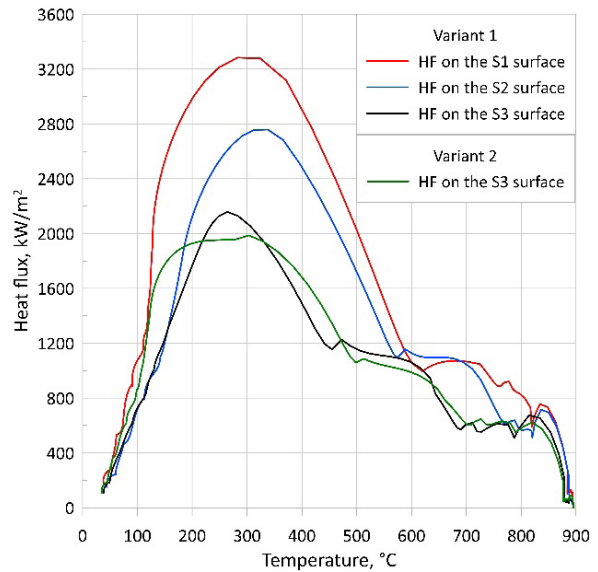


Fig. 10. Average HF values obtained in particular areas depending on the temperature of the cooled surface

The accuracy of the temperature field solution is presented in Table 2. The values of the average temperature deviation from the calculated ones using the inverse solution for both methods (variant 1 and variant 2) did not exceed 3K . The comparison of the temperature change obtained by the adopted solutions with the measurement (Figs. 11 and 12) shows that the greater convergence of the results was obtained by using the method that allows determining the boundary condition on the cooled surface as a function dependent on both position and time (variant 1). Determining the boundary conditions in the form of such a function allows determining the exact values of these conditions at a specific point on the cooled surface. The determination of the boundary conditions in the form of a function dependent only on time allows determining only the averaged values of the boundary conditions on the entire surface (area with radius r_3) at a given time. This solution does not reflect the actual conditions on the cooled surface. The nozzle design used in the research causes a change in the amount of liquid falling on the surface along the radius of the marked surface (Hadała et al., 2019). Therefore, the use of a method for calculating the local values of HTC and HF, depending on the local temperature (variant 1), allows not only to obtain greater accuracy of the solution but also a more accurate representation of the actual cooling process.

Table 2. The accuracy of the inverse solution

Variant	Average deviation [K]	Maximum negative deviation [K]	Maximum positive deviation [K]
1	1.977	-3.44	6.01
2	2.675	-4.08	8.89

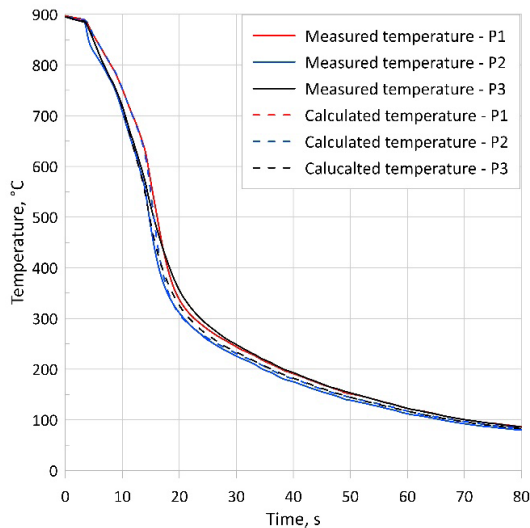


Fig. 11. Comparison of the temperature change determined from the inverse solution with that measured at P1, P2 and P3, variant 1

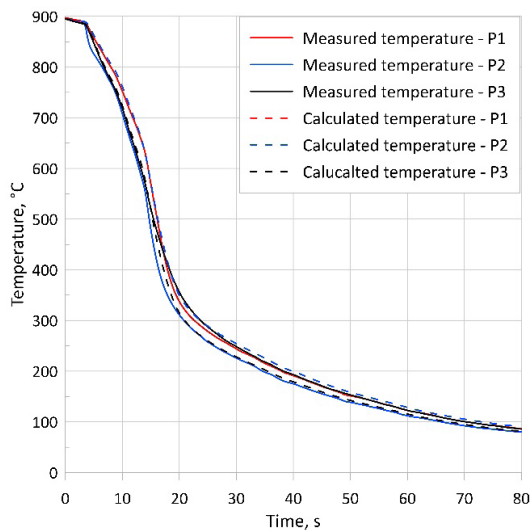


Fig. 12. Comparison of the temperature change determined from the inverse solution with that measured at P1, P2 and P3, variant 2

This method allows not only to determine the exact values of the boundary condition for a given point on the cooled surface but also the average values of the boundary condition in individual areas with radii r_1 , r_2 , and r_3 .

7. Conclusions

The boundary condition was identified in this paper on a water-cooled surface using two models of the approximation of the HTC on a cooled surface in the inverse solution. The identification was made on the basis of measuring the temperature change of the sensor cooled with a spray of water. The performed evaluation of the models showed satisfactory accuracy in both cases, the value of the average temperature deviation did not exceed 3 K. Depending on the model used in the inverse solution, there were some differences in the identified boundary conditions. The course of changes in the average values of HTC in the S3 area, determined by both variant 1 and variant 2, shows a large convergence during the film boiling. The differences appear in the range of the maximum HTC values. The results obtained by means of variant 1 at selected points showed the distribution of the boundary condition on the surface. This model reflects the actual surface conditions during cooling, resulting from the operation of the nozzle. The possibility of making the boundary condition dependent not only on time but also on the location allows for a more accurate description of the cooling process.

Acknowledgements

Scientific study financed from the regular activity of the Faculty of Metals Engineering and Industrial Computer Science of AGH University of Science and Technology. Work no. 16.16.110.663.

References

- Bellerová, H., Tseng, A.A., Pohanka, M., & Raudensky, M. (2012). Spray cooling by solid jet nozzles using alumina/water nanofluids. *International Journal of Thermal Sciences*, 62, 127–137.
- Broyden, C.G. (1970). The convergence of a class of double-rank minimization algorithms: 2. The new algorithm. *Journal of the Institute of Mathematics and its Applications*, 6, 222–231.
- Cebo-Rudnicka, A., Malinowski, Z., & Buczek, A. (2016). The influence of selected parameters of spray cooling and thermal conductivity on heat transfer coefficient. *International Journal of Thermal Sciences*, 110, 52–64.
- Edalatpour, S., Saboonchi, A., & Hassanpour, S. (2011). Effect of phase transformation latent heat on prediction accuracy of strip laminar cooling. *Journal of Materials Processing Technology*, 211(11), 1776–1782.
- Fletcher, R. (1970). A new approach to variable metric algorithms. *The Computer Journal*, 13(3), 317–322.
- Goldfarb, D. (1970). A family of variable-metric methods derived by variational means. *Mathematics of Computation*, 24(109), 23–26.
- Hadała, B., Malinowski, Z., Telejko, T., Szajding, A., & Cebo-Rudnicka, A. (2019). Experimental identification and a model of a local heat transfer coefficient for water – air assisted spray cooling of vertical low conductivity steel plates from high temperature. *International Journal of Thermal Sciences*, 136, 200–216.

- Huang, C.H., & Wang, S.P. (1999). A three-dimensional inverse heat conduction problem in estimating surface heat flux by conjugate gradient method. *International Journal of Heat and Mass Transfer*, 42(18), 3387–3404.
- Kim, H.K., & Oh, S.I. (2001). Evaluation of heat transfer coefficient during heat treatment by inverse analysis, *Journal of Materials Processing Technology*, 112(2–3), 157–165.
- Kręglewski, T., Rogowski, T., Ruszczyński, A., & Szymanowski, J. (1984). *Metody optymalizacji w języku FORTRAN* (J. Szymanowski, Red.), Wydawnictwo Naukowe PWN.
- Malinowski, Z. (2005). *Numeryczne modele w przeróbce plastycznej i wymianie ciepła*. Uczelniane Wydawnictwa Naukowo-Dydaktyczne AGH.
- PROMAT. *Karta katalogowa produktu PROMAFORM-1260*.
- Shanno, D.F. (1970). Conditioning of quasi-Newton methods for function minimization. *Mathematics of Computation*, 24(11), 647–656.
- Silk, E.A., Gollhofer, E.L., & Selvam, R.P. (2008). Spray cooling heat transfer: Technology overview and assessment of future challenges for micro-gravity application. *Energy Conversion and Management*, 49(3), 453–468.
- Steel work nozzles*. (n.d.). PNR. Retrieved May 24, from <https://www.pnr.co.uk/products/nozzles/spray-nozzles/steel-work-nozzles/>.
- Sun, C.G., Han, H.N., Lee, J.K., Jin, Y.S., & Hwang, S.M. (2002). A finite element model for the prediction of thermal and metallurgical behavior of strip on run-out-table in hot rolling. *ISIJ International*, 42(4), 392–400.
- Telejko, T., & Malinowski, Z. (2004). Application of an inverse solution to the thermal conductivity identification using the finite element method. *Journal of Materials Processing Technology*, 146(2), 145–155.
- Volle, F., Maillet, D., Gradeck, M., Kouachi, A., & Lebouché, M. (2009). Practical application of inverse heat conduction problem for wall condition estimation on rotating cylinder. *International Journal of Heat and Mass Transfer*, 52(1–2), 210–221.
- Zhou, J., Zhang, Y., Chen, J.K., & Feng, Z.C. (2012). Inverse estimation of front surface temperature of a plate with laser heating and convection-radiation cooling. *International Journal of Thermal Science*, 52, 22–30.
- Zienkiewicz, O.C., & Taylor, R.L. (2000). *The finite element method* (Vol. 1: *The basis*, Fifth Edition). Butterworth-Heinemann.

